# Electromagnetic Coupling Between a Thin-Wire Antenna and a Neighboring Biological Body: Theory and Experiment

KHALID KARIMULLAH, MEMBER, IEEE, KUN-MU CHEN, FELLOW, IEEE, AND DENNIS PAUL NYQUIST, MEMBER IEEE

*Abstract*—**Interaction between the near-zone EM field of a radiating antenna and a neighboring biological body is analyzed by considering the antenna current and the induced electric field in the body as unknown functions. A simultaneous pair of coupled, tensor integral equations is developed for these unknown functions. These equations are solved numerically by the method of moments using pulse function expansions for the unknowns and delta functions for testing. A monopole antenna coupled with a rectangular-cylindrical body model is used for the experimental verification of theoretical results. Accuracy of the numerical solution is substantiated by good agreement between the numerical and experimental results obtained for the antenna impedance and current distribution, as well as the induced electric field in the body. Electromagnetic (EM) radiation effects in various computer models of the human body are investigated to make a realistic assessment of potential radiation hazards associated with the coupled antenna-body system. It is found that an operator in the immediate vicinity of high-power transmitters may be exposed to harmful levels of radiation.**

## I. Introduction

THIS RESEARCH was performed to assess the potential biological hazard associated with back-pack or portable transmitters, CB radios, etc. Although the EM field excited in a biological body by plane-wave illumination has been successfully quantified [1]–[4], the interaction between the near-zone field of an antenna and a biological body is not well understood. Nyquist *et al.* [5] have studied this problem by assuming that the current distribution on the antenna is a known function. This assumption simplifies the problem considerably. Results obtained using this approach may not, however, be accurate for situations where the body is in near proximity to an antenna. The inaccuracy results from the fact that the current distribution on the antenna is perturbed by the EM field scattered by the biological body. This effect becomes very strong when the spacing between the antenna and body is small. In the theory presented here, the antenna current is no longer assumed known. The electric field induced in the body and the current distribution on the antenna are, therefore, both unknown functions. In other words, the antenna and the body are considered as a coupled system which is excited by a generator connected to the antenna.

A coupled antenna-body system consisting of a center-fed thin-wire dipole antenna adjacent to a conducting, polarizable body is analyzed. By using the image technique, this method can be extended to deal with thin-wire monopoles. A simultaneous pair of coupled, tensor integral equations is developed for the antenna current and the induced electric field in the body. These equations are solved numerically on a computer using the method of moments. Numerical results have been obtained for the induced electric field in the body, the antenna current, the antenna impedance, radiation-zone fields of the antenna-body system, the specific absorption rate (SAR) and the total power absorbed by the body.

Experiments have been conducted with a monopole antenna-body system operating at 600 MHz for which a plexiglass container filled with saline solution is used to simulate a biological body. Good agreement is achieved between the theoretical and experimental results for the impedance and current distribution of the antenna and the induced electric field in the body. A theoretical analysis of several realistic antenna-body models is made at 27 MHz, 80 MHz, and 90 MHz. The former is the CB radio frequency and the others are the near-resonant frequencies with respect to the height of a human adult. Several important observations drawn from this study are presented at the end of this paper.

## II. Theoretical Analysis

Simulation of the exact conditions that exist in practical situations, such as the operation of a CB radio or a back-pack transmitter, is very difficult. Initially, the case shown in Fig. 1, where an arbitrarily shaped, thin-wire antenna is closely coupled to a biological body of simple geometry, is analyzed. At a later stage it will be necessary to specialize this situation to that of Fig. 2 to achieve greater mathematical simplicity. This approach can also be extended to a monopole antenna-body system over an infinite ground plane.

Consider the situation of Fig. 1 where a biological body is exposed to the near-zone EM field of an antenna. As a result, conduction and polarization currents are induced in the body which depend upon the physiological parame-

Manuscript received April 8, 1980; revised July 18, 1980. This work was supported in part by the National Science Foundation under Grant ENG-74-12603 and Grant ECS-8001772, and in part by U. S. Army Research Office under Grant DAAG 29-76-G-0201.

The authors are with the Department of Electrical Engineering and System Science, Michigan State University, East Lansing, MI 48824.

0018-9480/80/1100-1218$00.75 ©1980 IEEE

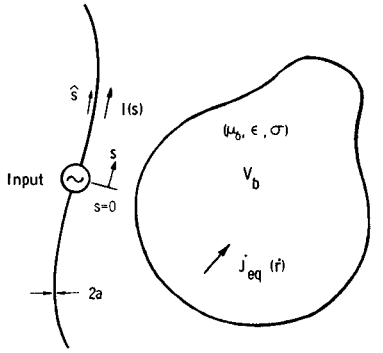


Fig. 1. A thin-wire antenna coupled to a biological body of volume $V_b$. This situation is also defined as antenna-body system.

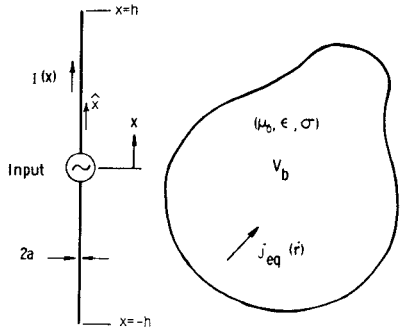


Fig. 2. A thin-wire, linear, center-fed dipole antenna coupled to a biological body of volume $V_b$.

ters, body geometry, the antenna-body configuration, and the frequency of the antenna. These induced currents in the body produce a scattered EM field. The total EM field in space is the sum of the incident field maintained by the antenna and the scattered field from the body. Since the current and charge on the antenna are always maintained in such a way as to satisfy the boundary conditions for $\vec{E}$ and $\vec{H}$ fields at the antenna surface, these quantities will be perturbed from their free-space values in the presence of a biological body. The perturbation in general becomes stronger as the antenna-body spacing is reduced.

For the system shown in Fig. 1, Maxwell's equations for all points in space exterior to the antenna are

$$\nabla\times\vec{E}(\vec{r})=-j\omega\mu_0\vec{H}(\vec{r}) \tag{1}$$

$$\nabla\times\vec{H}(\vec{r})=\sigma(\vec{r})\vec{E}(\vec{r})+j\omega\epsilon(\vec{r})\vec{E}(\vec{r}). \tag{2}$$

We assume that the total EM field in space is the sum of two fields

$\{\vec{E}^a, \vec{H}^a\}$ = incident EM field of the antenna

$\{\vec{E}^b, \vec{H}^b\}$ = scattered EM field from the biological body.

Therefore

$$\vec{E}(\vec{r})=\vec{E}^a(\vec{r})+\vec{E}^b(\vec{r}) \tag{3}$$

$$\vec{H}(\vec{r})=\vec{H}^a(\vec{r})+\vec{H}^b(\vec{r}). \tag{4}$$

For points exterior to the antenna, we will have the following equations for the incident EM field

$$\nabla\times\vec{E}^a(\vec{r})=-j\omega\mu_0\vec{H}^a(\vec{r}) \tag{5}$$

$$\nabla\times\vec{H}^a(\vec{r})=j\omega\epsilon_0\vec{E}^a(\vec{r}). \tag{6}$$

Similarly, for the scattered field from the body we can write

$$\nabla\times\vec{E}^b(\vec{r})=-j\omega\mu_0\vec{H}^b(\vec{r}) \tag{7}$$

$$\nabla\times\vec{H}^b(\vec{r})=\vec{J}_{eq}(\vec{r})+j\omega\epsilon_0\vec{E}^b(\vec{r}) \tag{8}$$

with the condition that (1) and (2) are satisfied identically. By using (6), (8) and superposition, (2) is satisfied with

$$\vec{J}_{eq}(\vec{r})=\tau(\vec{r})\vec{E}(\vec{r})=\text{equivalent current density} \tag{9}$$

which describes induced conduction and polarization currents immersed in unbounded free space, where

$$\tau(\vec{r})\equiv\sigma(\vec{r})+j\omega\{\epsilon(\vec{r})-\epsilon_0\}=\text{complex conductivity}. \tag{10}$$

The solutions for the incident electric field from the antenna and the scattered electric field from the biological body, using free-space tensor Green's function [6], are written as

$$\vec{E}^a(\vec{r})=\int_{\text{ant}} I(s')\hat{s}'\cdot\vec{\vec{G}}(\vec{r},s')\,ds' \tag{11}$$

$$\vec{E}^b(\vec{r})=\text{PV}\int_{V_b}\vec{J}_{eq}(\vec{r}')\cdot\vec{\vec{G}}(\vec{r},\vec{r}')\,dV'-\frac{\vec{\vec{I}}\cdot\vec{J}_{eq}(\vec{r})}{3j\omega\epsilon_0} \tag{12}$$

where $\vec{\vec{I}}$ = the identity tensor; $\vec{\vec{G}}(\vec{r},\vec{r}')=-j\omega\mu_0[\vec{\vec{I}}+\nabla\nabla/k_0^2]G_0(\vec{r},\vec{r}')$ = tensor Green's function; $G_0(\vec{r},\vec{r}')=\exp(-jk_0|\vec{r}-\vec{r}'|)/4\pi|\vec{r}-\vec{r}'|$; $k_0=\omega\sqrt{\mu_0\epsilon_0}$; $\vec{r}$ is a field point; $\vec{r}'$ is a source point interior to $V_b$; $s'$ is a source point along the antenna axis; and $\hat{s}'$ is a unit vector in the axial direction at $s'$. The symbol PV denotes the principal value of the integral carried out by excluding an infinitesimally small volume surrounding the field point. For point $\vec{r}$ exterior to $V_b$, the field in (12) is given by the tensor integral only. Using (3), (11), and (12) we obtain the following tensor integral equation:

$$\left\{1+\frac{\tau(\vec{r})}{3j\omega\epsilon_0}\right\}\vec{E}(\vec{r})-\text{PV}\int_{V_b}\tau(\vec{r}')\vec{E}(\vec{r}')\cdot\vec{\vec{G}}(\vec{r},\vec{r}')\,dV'=\int_{\text{ant}} I(s')\hat{s}'\cdot\vec{\vec{G}}(\vec{r},s')\,ds' \tag{13}$$

where $\vec{r}$ locates a point inside $V_b$.

Next we satisfy the boundary condition for the $\vec{E}$ field at the surface of the antenna. The boundary condition for tangential field at points along the surface of the perfectly conducting antenna excited by a slice generator leads to

$$\hat{s}\cdot\{\vec{E}^a(s)+\vec{E}^b(s)\}=-V_0\delta(s) \tag{14}$$

where $V_0$ is the driving-point input voltage, $s$ is a field point on the antenna surface, and $\hat{s}$ is a unit vector at $s$ tangential to the antenna surface. Consequently, we obtain

$$\hat{s}\cdot\int_{\text{ant}} I(s')\hat{s}'\cdot\vec{\vec{G}}(s,s')\,ds'+\hat{s}\cdot\int_{V_b}\tau(\vec{r}')\vec{E}(\vec{r}')\cdot\vec{\vec{G}}(s,\vec{r}')\,dV'=-V_0\delta(s). \tag{15}$$

Equation (13) yields three scalar integral equations while

(15) is a fourth such equation. We can establish the uniqueness of the solution by noting that there are four coupled unknown functions described by four simultaneous integral equations.

The solutions for induced electric field in the body and antenna current, obtained through (13) and (15), are dependent upon how accurately the delta function can be approximated in numerical analysis. However, in the case of a linear dipole antenna, we can overcome this problem effectively by exploiting the Hallen-type integral-equation formulation for the antenna current [7]. Consider the configuration of Fig. 2. The vector potential at the surface of the antenna, maintained exclusively by the antenna current, can be approximated by

$$A_x^a(x)=\frac{\mu_0}{4\pi}\int_{-h}^{h} I(x')K_a(x,x')\,dx' \tag{16}$$

where

$I(x')$ antenna current;

$K_a(x,x')$ $\exp(-jk_0R)/R$;

$R=\{(x-x')^2+a^2\}^{1/2}$

$x'$ a source point along the antenna axis; and

$x$ a field point at its surface.

This approximation is valid for thin-wire antennas. Similarly, the line charge density will produce scalar potential $\phi^a(x)$. Using the Helmholtz integral for $\phi^a(x)$, the continuity equation and the boundary conditions $I(h)=I(-h)=0$, one can easily obtain

$$\phi^a(x)=\frac{j}{4\pi\epsilon_0\omega}\frac{\partial}{\partial x}\int_{-h}^{h} I(x')K_a(x,x')\,dx'. \tag{17}$$

Since

$$E_x^a(x)=-\frac{\partial\phi^a(x)}{\partial x}-j\omega A_x^a(x)$$

we can use (16) and (17), as well as the boundary condition for the electric field at the surface of the antenna, to obtain

$$\left(\frac{\partial^2}{\partial x^2}+k_0^2\right)\int_{-h}^{h} I(x')K_a(x,x')\,dx' = -\frac{j4\pi k_0}{\eta_0}\{V_0\delta(x)+E_x^b(x)\} \tag{18}$$

where $\eta_0=\sqrt{\mu_0/\epsilon_0}$ and $E_x^b(x)$ is the $x$-component of the scattered electric field at the surface of the antenna due to induced conduction and polarization currents in the biological body. Using Lagrange's variational method, the solution to (18) is obtained as

$$\int_{-h}^{h} I(x')K_a(x,x')\,dx+A\cos k_0x+B\sin k_0x +j\frac{4\pi}{\eta_0}\int_0^x E_x^b(u)\sin k_0(x-u)\,du = -j\frac{2\pi}{\eta_0}V_0\sin k_0|x| \tag{19}$$

where $x$ locates a point on the antenna surface.

Equation (19) is Hallen's integral equation for the antenna current with an additional forcing function due to the term involving $E_x^b$. Finally, for the case shown in Fig. 2, (13) can be written as

$$\left\{1+\frac{\tau(\vec{r})}{3j\omega\epsilon_0}\right\}\vec{E}(\vec{r})-\mathrm{PV}\int_{V_b}\tau(\vec{r}')\vec{E}(\vec{r}')\overleftrightarrow{G}(\vec{r},\vec{r}')\,dv' = \int_{-h}^{h} I(x')\hat{x}\cdot\overleftrightarrow{G}(\vec{r},x')\,dx' \tag{20}$$

where $\vec{r}$ locates any point inside $V_b$. Equations (19) and (20) are solved numerically by the method of moments. The antenna is partitioned into $N_a$ segments and the body is subdivided into $N_b$ subvolumes. Pulse function expansions are used to approximate the antenna current and the induced electric field in the body as

$$I(x)=\sum_{l=1}^{N_a} I_l p_l(x) \qquad \vec{E}(\vec{r})=\sum_{n=1}^{N_b}\vec{E}^n p_n(\vec{r})$$

where

$I_l$ antenna current at the $l$th partition;

$\vec{E}^n$ induced electric field in the $n$th subvolume

$$p_l(x)=\begin{cases}1, & x \text{ in } (\Delta x)_l\\ 0, & \text{otherwise}\end{cases} \qquad p_n(\vec{r})=\begin{cases}1, & \vec{r} \text{ in } (\Delta V)_n\\ 0, & \text{otherwise.}\end{cases}$$

$(\Delta x)_l$ and $(\Delta V)_n$ represent the $l$th segment of the antenna and the $n$th subvolume of the body, respectively. Point matching (19) at each partition of the antenna and equation (20) in each subvolume of the body, subsequent to exploiting the pulse function expansions, leads to a system of linear algebraic equations for unknown currents and fields. This system is demonstrated below:

$$\begin{array}{c} \\ N_a \\ 3N_b \end{array}\begin{array}{c} \begin{array}{cc} N_a & 3N_b \end{array} \\ \left[\begin{array}{c|c} I-I & E-I \\ \hline I-E & E-E \end{array}\right] \end{array}\left[\begin{array}{c} I_l \\ \hline E_x^n \\ E_y^n \\ E_z^n \end{array}\right]=\left[\begin{array}{c} V_0f(x_l) \\ \hline 0 \end{array}\right]$$

where $f(x_l)=-(j2\pi/\eta_0)\sin k_0|x_l|$, and $x_l$ is the central coordinate of the $l$th segment. The elements of the $(N_a+3N_b)\times(N_a+3N_b)$ matrix are available elsewhere [8]. These equations are solved numerically by digital computer. Once the antenna current and the induced electric field in the body are known, the antenna impedance, the absorbed power density, the radiation-zone field, etc., are easily computed.

## III. Experimental Study

Experiments were conducted to verify the numerical results obtained from the computer program. A 600-MHz monopole antenna-body system was chosen for this study. A rectangular cylindrical plexiglass container of dimensions 12.5 cm×6.25 cm×1.56 cm filled with 0.5 N saline solution was used to replicate a biological body. A general experimental setup and the corresponding computer model is shown in Fig. 3. This study consists of three distinct parts.

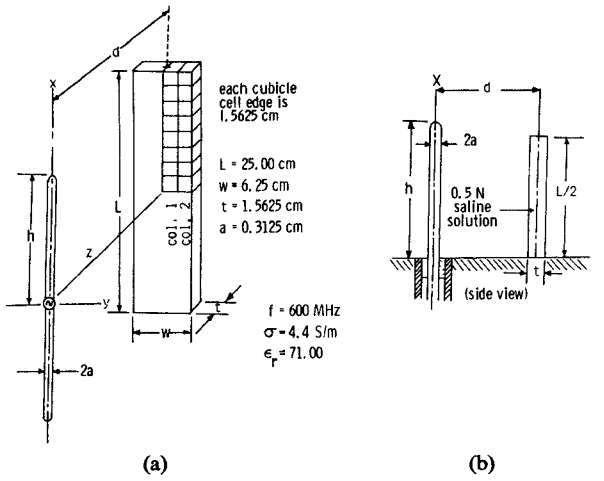


Fig. 3. (a) The theoretical model and (b) the corresponding geometrical setup used in the computer-aided numerical solution.

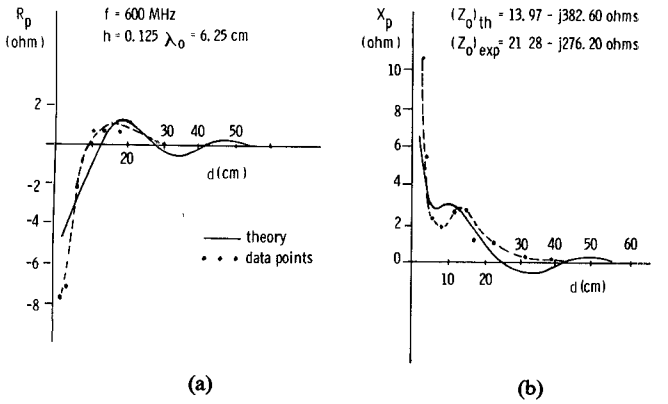


Fig. 4. Perturbation ($Z_p = R_p + jX_p$) in input impedance versus the spacing $d$ between the antenna and the body. $Z_p = Z_{in} - Z_0$, $Z_{in}$ = input impedance of the antenna with coupling and $Z_0$ = the free-space impedance. (a) Perturbation $R_p$ to antenna resistance. (b) Perturbation $X_p$ to antenna resistance.

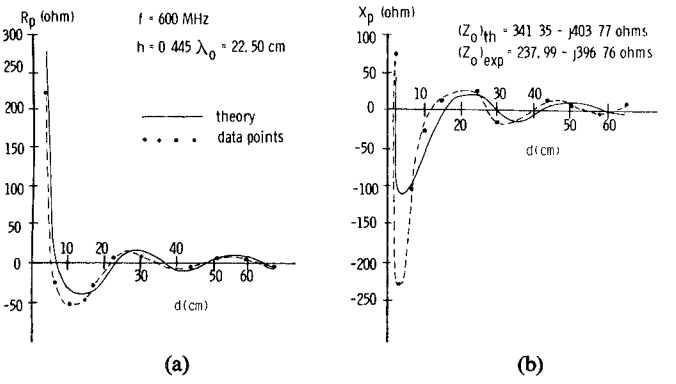


Fig. 5. Perturbation ($Z_p = R_p + jX_p$) in input impedance versus the spacing $d$ between the antenna and the body. $Z_p = Z_{in} - Z_0$, $Z_{in}$ = the input impedance of the antenna with coupling and $Z_0$ = the free-space impedance. (a) Perturbation $R_p$ to antenna resistance. (b) Perturbation $X_p$ to antenna resistance.

### *A. Perturbation to Input Impedance of the Antenna*

A biological body in the neighborhood of an antenna affects the antenna impedance. The perturbation $Z_p$ in the input impedance of the antenna is defined by $Z_p = Z_{in} - Z_0$, where $Z_0$ is the impedance of the antenna immersed in unbounded free space, and $Z_{in}$ is its impedance when a biological body is placed in close proximity.

The input impedance is measured by using a vector voltmeter [8]. Induced voltages from an electric field probe and a magnetic field probe installed in the feeding coaxial waveguide are measured by the voltmeter. The complex ratio of these phasor voltages (using predetermined calibration factor) gives the input impedance at the probe location. This impedance is finally transformed to the driving-point impedance.

The perturbation $Z_p$ is plotted as a function of the spacing between antenna and body. The results are shown in Figs. 4 and 5, respectively, for a short monopole and a near-antiresonant-length monopole. There is good agreement between theory and experiment, especially for antenna-body spacings greater than 10 cm. For smaller spacings, the trend in variations is in good agreement. In this region, the electric field is a rapidly changing spatial function and we therefore expect some inaccuracy in the results due to relatively-slow convergence of the numerical solution.

### *B. Antenna Current Distribution*

The current distribution along the antenna is measured by an $H$-field probe which transduces a voltage induced by the magnetic field at the surface of the antenna; this voltage is thus proportional to the antenna current. Construction of the probe is based on the technique employed by King [7]. Current distributions in free space and in the presence of the biological body are indicated for quarter-wavelength and near-antiresonant monopoles in Figs. 6 and 7. Normalized antenna current distributions have been plotted, where the maximum value of the corresponding free-space distribution is used for normalization. There is a remarkable agreement between theory and experiment. The current distribution along the longer monopole is distinctly different from the free-space distribution, a significant observation.

### *C. Induced Electric Field in the Body*

In order to determine the induced electric field in the body, the first step is to replace the saline solution by a synthetic jelly-like substance commonly referred to as phantom material. The conductivity of this compound is determined by its salt content. One face of the container is slotted to receive the electric field probe, so that field is measurable along two columns (col. 1 and col. 2 shown in Fig. 3). The probe has been designed specifically for $\vec{E}$-field measurements inside biological systems [9]. The results of experiments are compared with theory in Fig. 8. Relative values of the electric field are plotted as a function of the vertical displacement along the two columns. There is good agreement between theory and experiment. A prominent effect verified experimentally for this case is that the field in the outer column is greater than that in the inner column.

Experimental accuracy of all the above methods was

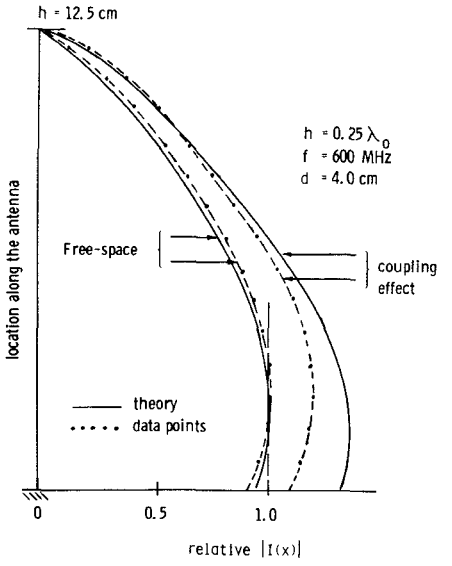


Fig. 6. EM coupling effect on the antenna current distribution for an antenna of height $h=\lambda_0/4$. Geometry and electrical parameters correspond to Fig. 3.

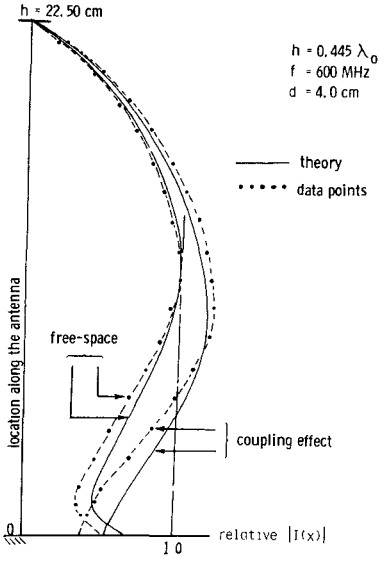


Fig. 7. EM coupling effect on the antenna current distribution for an antenna of height $h=0.445\lambda_0$. Geometry and electrical parameters correspond to Fig. 3.

verified by comparing the theoretical and experimental results obtained for the antenna impedance, the antenna current and the near-zone electric field of a monopole in free-space. Very good agreement was achieved for each of the above quantities.

## IV. Study of Some Antenna-Body Computer Models

In this section some important antenna-body coupling problems are solved numerically. Firstly, we have studied an antenna-body system with a rectangular-cylindrical body and a quarter-wavelength dipole (or monopole for grounded systems). The dimensions and weight of the model have been chosen to approximate that

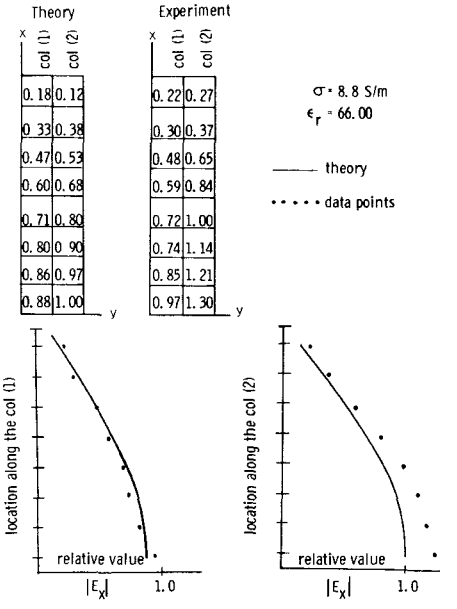


Fig. 8. Distribution of induced electric fields inside the biological body of Fig. 3 when irradiated by the impressed field from the antenna of height $h=0.25\lambda_0$ at 600 MHz.

of a human adult. Secondly, we have attempted to determine the nonsymmetric current distribution anticipated when an antenna is located asymmetrically with respect to the body. Thirdly, the radiation field pattern of some antenna-body systems have been plotted and, finally, the case of an antenna coupled to a realistic human-body model has been investigated.

### A. 27-MHz Antenna-Body System

A rectangular body of dimensions 170 cm×20 cm×20 cm and an antenna of height $h=2.77$ m is chosen. The system is operated at 27 MHz, the CB radio frequency. Conductivity and relative permittivity of the body are 0.62 S/m and 113.0, respectively. The weight of the body is 150 lb (68 kg). In Fig. 9 an isolated antenna-body system is indicated. The specific absorption rate (SAR) and the induced electric field are indicated at each cell location, based on antenna input power of 1 W. The total power absorbed by the body is 0.00644 W. In Fig. 10, a quarter-wavelength, monopole antenna illuminates the same biological body which is now in direct contact with ground. In this case the power absorbed is 0.084 W, nearly 14 times that of the previous example. Nearly 8.5 percent of the antenna input power, therefore, is absorbed by the body when it is in direct contact with ground.

The numerical accuracy of our computer program is tested using this model. In Fig. 9, if the body is placed very far from the antenna, then 1) the impressed EM field will be approximately a transverse plane wave in the region that forms the biological body, and 2) the antenna and body will be essentially uncoupled so the antenna current will be essentially the free-space current which, to a first approximation, can be assumed sinusoidal.

In the test, the value of the driving current at the antenna input is determined, based on the sinusoidal current assumption, such that an impressed radiation in-

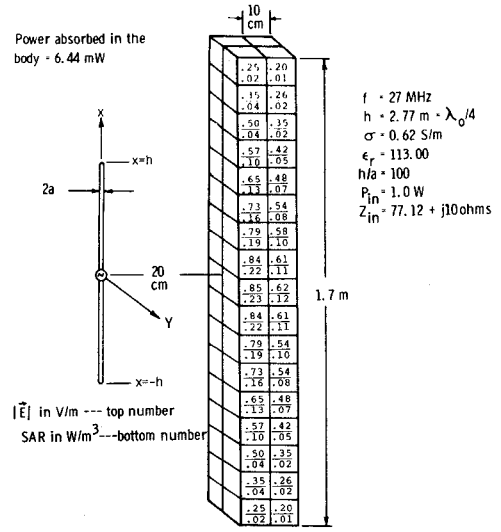


Fig. 9. Distribution of induced electric fields and the specific absorption rate at the central location of each cell of the body for an isolated antenna-body system. Antenna is driven by an input power of 1 W.

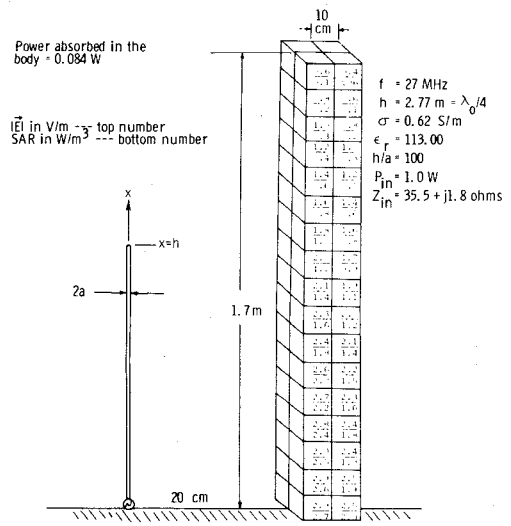


Fig. 10. Distribution of induced electric fields and the specific absorption rate at the central location of each cell of the body for an antenna-body system over infinite ground plane. Antenna is driven by an input power of 1 W.

tensity of 10 mW/cm$^2$ is produced at 100 m from the antenna. Next, the body is placed at this location, according to the geometry of Fig. 9, and the antenna-body coupling problem is solved using our computer program. The power absorbed in the body, with the driving current of the antenna set to the above-determined value, is found to be 11.65 W. This figure agrees very well with the 12 W predicted by Massaudi *et al.* [4] for a body of similar dimensions irradiated by a 10 mW/cm$^2$ uniform plane wave.

The manner in which the power absorbed by the body varies with the antenna-body spacing is best described by Fig. 11. In this figure, the power $P_a$ (watts) absorbed by the body has been indicated as a function of $(d/d_m)$ on a log–log graph. $d$ is the spacing between the antenna and the body and $d_m$ is the minimum spacing, which in our analysis is 0.25 m. Three configurations are studied. Curve

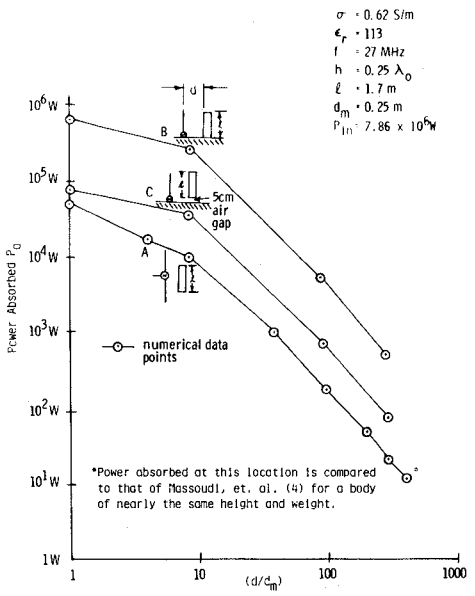


Fig. 11. Power absorbed in the body versus the antenna-body spacing for the 27-MHz antenna-body systems. The height of the body is 1.7 m and its weight is approximately 150 lb.

*A* represents the isolated antenna-body system of Fig. 9, curve *B* represents the monopole-body system of Fig. 10, and curve *C* represents a monopole-body system similar to that in Fig. 10 with the body separated from ground by a 5-cm air-insulation gap. In all cases, the values of the absorbed power are *relative* in the sense that they are based on a fixed value of antenna input power. Even though the choice of antenna input power is arbitrary we have chosen the fixed input power as the power needed to produce 10 mW/cm$^2$ intensity at 100 m from the dipole antenna in free space. This choice enables us to compare the absorbed powers for various antenna-body configurations and spacings to the 11.65-W figure at 100-m spacing, which was itself compared to the result of Massoudi *et al.* [4].

### *B. 90-MHz Antenna-Body System*

A human-body model of an average adult (height = 1.7 m and weight 179 lb) is chosen for investigation of electromagnetic coupling effects. The conductivity inside the body is assumed uniform. The coupling problem based on a quarter-wave monopole interacting with the body over infinite ground is formulated. The results, which are based on antenna-body spacing of 20 cm, are presented in Fig. 12. The absorbed power is 0.5216 W when the power input to antenna is 1 W. This strong coupling is due to the fact that at 90 MHz the body achieves a near-resonant condition. In such a situation, more than 50 percent of the input power is absorbed by the body. Furthermore, it is observed that greater absorption occurs in the legs.

### *C. 80-MHz Antenna-Body System*

This system is indicated in Fig. 13(a). The shape of the body has the approximate appearance of a human adult. The objectives are to determine the effects of coupling upon the current distribution along an antenna in near

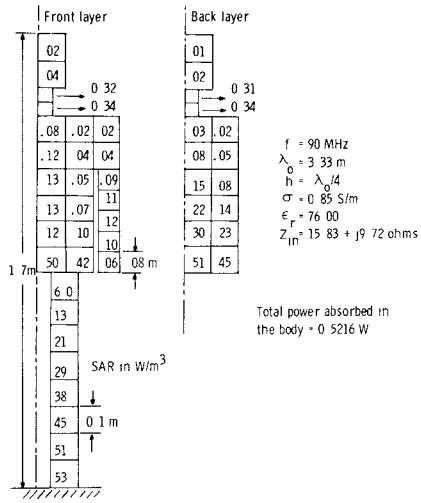


Fig. 12. Distribution of the specific absorption rate inside the realistic model of man located in the immediate vicinity of a grounded quarter-wave monopole antenna. Values are based on input power of 1.0 W and spacing of 20 cm between the dipole and the antenna.

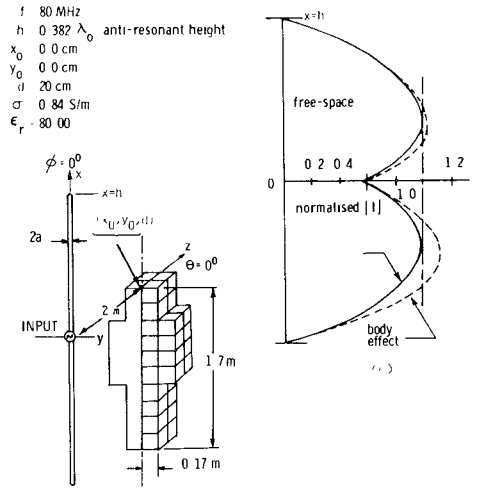


Fig. 13. The 80-MHz antenna-body system using a near-antiresonant length antenna at 80 MHz. (a) Antenna-body system configuration showing the center of the antenna located at top-of-head level. (b) Current distribution of antenna in presence of body and in free space when $h$ is near antiresonant length.

proximity to a biological body, and to predict the radiation pattern maintained by this antenna-body system. Uniform conductivity and permittivity is assumed. For the first objective, an antenna of half-length $0.382\lambda_0$ is chosen, where $\lambda_0$ is the free-space wavelength. The center of the antenna is located at head level as shown in Fig. 13(a), and the antenna-body spacing is maintained at 20 cm. The current distribution calculated numerically for this system is indicated in Fig. 13(b). The current distribution on the antenna is no longer symmetric. This effect is not as strong for antennas with $h<\lambda_0/4$. The radiation patterns maintained by antenna-body systems consisting of the same body but with antenna heights of $h=0.125\lambda_0$ and $h=0.25\lambda_0$ are presented in Fig. 14. The presence of a body at 20 cm provides a system effect similar to that

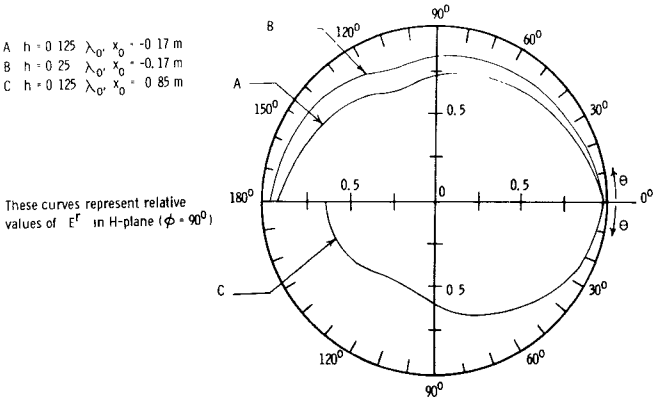


Fig. 14. Radiation field pattern maintained by dipole antenna coupled to the human body model in $H$-plane of the dipole (geometry, dimensions and parameters are same as in Fig. 13(a)).

obtained when a director element is used in a parasitic antenna array. These patterns are indeed dependent upon the antenna height, the frequency, the spacing and the geometrical configuration of the antenna-body system.

## V. Summary

The scope of this study includes an analytical and experimental investigation of the following phenomena: 1) the current distribution on an antenna located in near proximity to a conducting, polarizable biological body; 2) the perturbation to the input impedance to the antenna due to the neighboring biological body; and 3) the induced electric field distribution inside the body.

Experimental verification of three primary aspects of the theory developed in Section II was made, and the results were found to be in good agreement. Numerical accuracy of the analytical method used to solve the coupled, integral equations for the field inside the body and the current on the antenna was tested on a cylindrical model of height 1.7 m and weight 150 lb. This was accomplished at a frequency of 27 MHz, which is the CB radio operating frequency.

Results from the above test and the experiments carried out in this study provide a high level of confidence in predictions made on the basis of the numerical results. The important observations drawn by analyzing various antenna-body systems (which contain biological bodies of human-adult size) can be summarized as follows.

1) EM-coupling is increased considerably when a body is allowed to make direct contact with the ground (compared to bodies isolated from ground).
2) About 8.5 percent of the input power is absorbed by an average human adult while standing at a distance of 20 cm from a quarter wave antenna operating at 27 MHz.
3) If a frequency of 90 MHz (which makes the adult height nearly equal to a resonant length) is used, slightly over 50 percent of the input power is absorbed by the body spaced 20 cm from the antenna.

4) The power absorbed by a human adult standing at a distance of 20 cm from the antenna when its input power is 30 W (140 W) at 90 MHz (27 MHz) is the same as the power that would be absorbed from the exposure to 10-mW/cm$^2$ plane-wave irradiation.
5) For antennas of height $h>\lambda_0/4$, the current is perturbed quite appreciably from its free-space distribution when in near proximity to a biological body. Also, a nonsymmetric antenna-body configuration produces a nonsymmetric antenna current distribution.
6) The body may act as a director element when placed close to an antenna. This has been demonstrated in the case of an 80-MHz antenna-body system.

## References

[1] D. Livesay and K. M. Chen, "Electromagnetic field induced inside arbitrarily shaped biological bodies," *IEEE Trans. Microwave Theory Tech.*, vol. MTT-22, pp. 1273–1280, Dec. 1974.
[2] K. M. Chen and B. S. Guru, "Induced EM fields inside human bodies irradiated by EM waves of up to 500 MHz," *J. Microwave Power*, vol. 12, no. 2, pp. 173–183, 1977.
[3] M. J. Hagmann, O. P. Gandhi, and C. H. Durney, "Numerical calculation of electromagnetic disposition for a realistic model of man," *IEEE Trans. Microwave Theory Tech.*, vol. MTT-27, pp. 804–809, Sept. 1979.
[4] H. Massoudi, C. H. Durney, and C. C. Johnson, "Long-wave-length EM power absorption in ellipsoidal model of man and animals," *IEEE Trans. Microwave Theory Tech.*, vol. MTT-25, pp. 47–52, Jan. 1977.
[5] D. P. Nyquist, K. M. Chen, and B. S. Guru, "Coupling between small thin-wire antennas and a biological body," *IEEE Trans. Antennas Propagat.*, vol. AP-25, pp. 863–866, Nov. 1977.
[6] J. Van Bladel, "Some remarks on Green's dyadic for infinite space," *IRE Trans. Antennas Propagat.*, vol. AP-9, pp. 563–566, Nov. 1961.
[7] R. W. P. King, *Theory of Linear Antennas*. Cambridge, MA: Harvard Univ. Press, 1956, pp. 251–252.
[8] K. Karimullah, "Theoretical and experimental study of the proximity effects of thin-wire antenna in presence of biological bodies," Ph.D. dissertation, Michigan State Univ., East Lansing, MI, 1979.
[9] K. M. Chen, S. Rukspollmuang, and D. P. Nyquist, "Measurement of induced electric fields in a phantom model of man," presented at Int. Symp. Biological Effects of Electromagnetic Waves, (Helsinki, Finland), July 31, 1978–Aug. 8, 1978.

# Short Papers

## On the Odd-Mode Capacitance of the Coupled Microstriplines

S. S. BEDAIR

*Abstract*—**This short paper aims to recognize the correct decomposition for the total odd-mode capacitance of the coupled microstriplines and present an improved expression for the gap capacitances. The used procedure utilizes the results which were obtained earlier by the conformal mapping techniques.**

### I. Introduction

In recent years, a number of papers have reported the use of single microstripline as an intermediate step for designing coupled microstriplines [2]–[5]. Garg and Bahl [5] successfully used an approach to obtain coupled capacitances by suitably dividing the total capacitance into a parallel plate and fringing ones. The design equations presented by Garg and Bahl [5] are believed to be the most accurate so far. However, in these equations the decomposition of the total odd-mode capacitance is not in accordance with electromagnetic field theory, in that the basic capacitances $C_{10}$ and $C_{12}$ in Fig. 1(a) are not functions of the applied voltage on any of the conductors [1]. Therefore, the even-mode capacitance must appear in the expression for the odd-mode capacitance Fig. 1(b).

Manuscript received April 29, 1980; revised July 10, 1980.
The author is with the Electronics Laboratory, The University of Kent at Canterbury, Canterbury, Kent, CT2 7NT, U.K., on leave from the Military Technical College, Cairo, Egypt.

### II. Calculation of the Odd-Mode Capacitance

The breakup of the odd-mode capacitance into parallel plate fringing and gap capacitances is shown in Fig. 2. The odd-mode capacitance may be written as

$$C_o = C_p + C_f + C_f' + C_{ga} + C_{gd} \quad (1)$$

where $C_p$, $C_f$, and $C_f'$ are the same as those given by Garg and Bahl [5]. $C_{gd}$ may be calculated exactly using the results obtained for the corresponding coupled striplines shown in Fig. 3, except

0018-9480/80/1100-1225$00.75 ©1980 IEEE